Summer 8-2024

Modelling Three Dimensional Morphology of Retinal Pigment Epithelium

Akinwale Famotire

Modelling Three Dimensional Morphology of Retinal Pigment Epithelium

by

Akinwale Victor Famotire

Under the Direction of Yi Jiang, Ph.D.

A Thesis Submitted in Partial Fulfillment of the Requirements for the Degree of

Master of Science

in the College of Arts and Sciences

Georgia State University

2024

ABSTRACT

Age-related macular degeneration (AMD) is the primary cause of vision loss in Americans over 65. The retinal pigment epithelium (RPE) is essential for photoreceptor cell health, and its dysfunction is an early AMD indicator. Although RPE shape changes are observed in AMD conditions, detailed morphological understanding is limited. State-of- the-art morphometric analysis focuses on the apical surface in 2D, missing true physiological dynamics. 3D experimental observations of RPE and Corneal Endothelial Cells (CECs) which exhibit similar patterns to RPE, revealed basal infolding and interdigitation, respectively. We developed a computational model using the Cellular Potts Model (CPM) to represent RPE cells in 3D, investigating the biophysical mechanisms of these features. Our findings reveal that cell-cell and cell-matrix adhesion interactions, along with geometric constraints, drive these morphological changes. Variations in adhesion properties significantly affect cellular morphology and organization, and their interplay with geometric constraints results in the observed interdigitation and infolding patterns.

INDEX WORDS: AMD, RPE, CSM, CPM, 3D MODELLING, CECs

Modelling Three Dimensional Morphology of Retinal Pigment Epithelium

by

Akinwale Victor Famotire

Committee Chair: Yi Jiang

Committee: Jun Kong

Datta Sayantan

Electronic Version Approved:

Office of Graduate Services

College of Arts and Sciences

Georgia State University

August 2024

DEDICATION

This work is dedicated to the Almighty God for the grace and strength that enabled me to complete this project

ACKNOWLEDGMENTS

I express my profound gratitude to God for the opportunity, grace, and the precious gift of life bestowed upon me throughout this Master's program.

My journey has been enriched by the guidance of my supervisor, Professor Yi Jiang. I am truly grateful for the immeasurable impact she has had on my academic and personal growth. Her mentorship and expertise have been invaluable, shaping my understanding, research skills and projecting me for future works. I am indebted to Professor Yi Jiang for her unwavering support and dedication to my success.

Additionally, I would like to express my gratitude to the Compucell3D team, especially Dr. James Sluka, for the immense support and help offered during the computational setup of this project and providing responses to every of my questions and problems encountered.

I extend my sincere appreciation to my lab mate, Somiya Rauf, for her time and support, and also for the insights from other lab mates, including Caleb Hightower, Sima Moshafi, Sheriff Akeeb, Isaac Godspeed, to mention a few. My gratitude also goes to the Graduate Coordinators of the Department of Mathematics and Statistics, Dr. Zhongshan Li and Dr. Gengsheng Qin, as well as the entire staff of the department for their unwavering support.

This acknowledgment would be incomplete if I fail to recognize my family: my loving mother and father, Agnes M. Famotire and Akinyemi Famotire, and my siblings, Favour and Felix. I am also deeply grateful to my pastors, Dr. Ayoola Naths and his family, and Pastor Olaniyi and his family, for their unwavering support.

TABLE OF CONTENTS

LIST OF TABLES

LIST OF FIGURES

CHAPTER 1
INTRODUCTION

1.1 Background of the Study

The Retinal Pigment Epithelium (RPE) is a single layer of cell located between the photoreceptors of the retina and blood vessels of the choroid. Figure 1.1 (adapted from (1)) shows the anatomical structure of the eye focusing on the macula to depict the position of the RPE. In healthy eyes, the RPE is a single sheet of densely packed hexagonal cells that performs crucial functions such as acting as a barrier between the retina and choroid, light absorption, supplying nutrients to photoreceptors, controlling ion homeostasis, eliminating water and metabolites from the outer retina to choroid (2). Thus, the degeneration of the RPE can have a profound impact on visual acuity leading to several eye conditions, some of which might cause vision impairment or total blindness (3). Some examples of eye defects caused by degeneration of this organ include: retinitis pigmentosa, age-related macular degeneration (AMD), stargardt disease (SD), choroideremia and bestrophinopathies.

Age-related Macular Degeneration (AMD) is one of the most common eye condition caused by the dysfunction of the RPE cell. It is a leading cause of vision impairment worldwide among persons 65 years and older in industrialized countries (4). AMD manifests as a progressive deterioration of the macular, the central part of the retina responsible for sharp, central vision. As an age-related disease, the prevalence of AMD increases with age affecting approximately 19.8 million Americans aged 40 and older (5) . The earliest stage of the disease is asymptomatic and is usually diagnosed when extracellular aggregates called

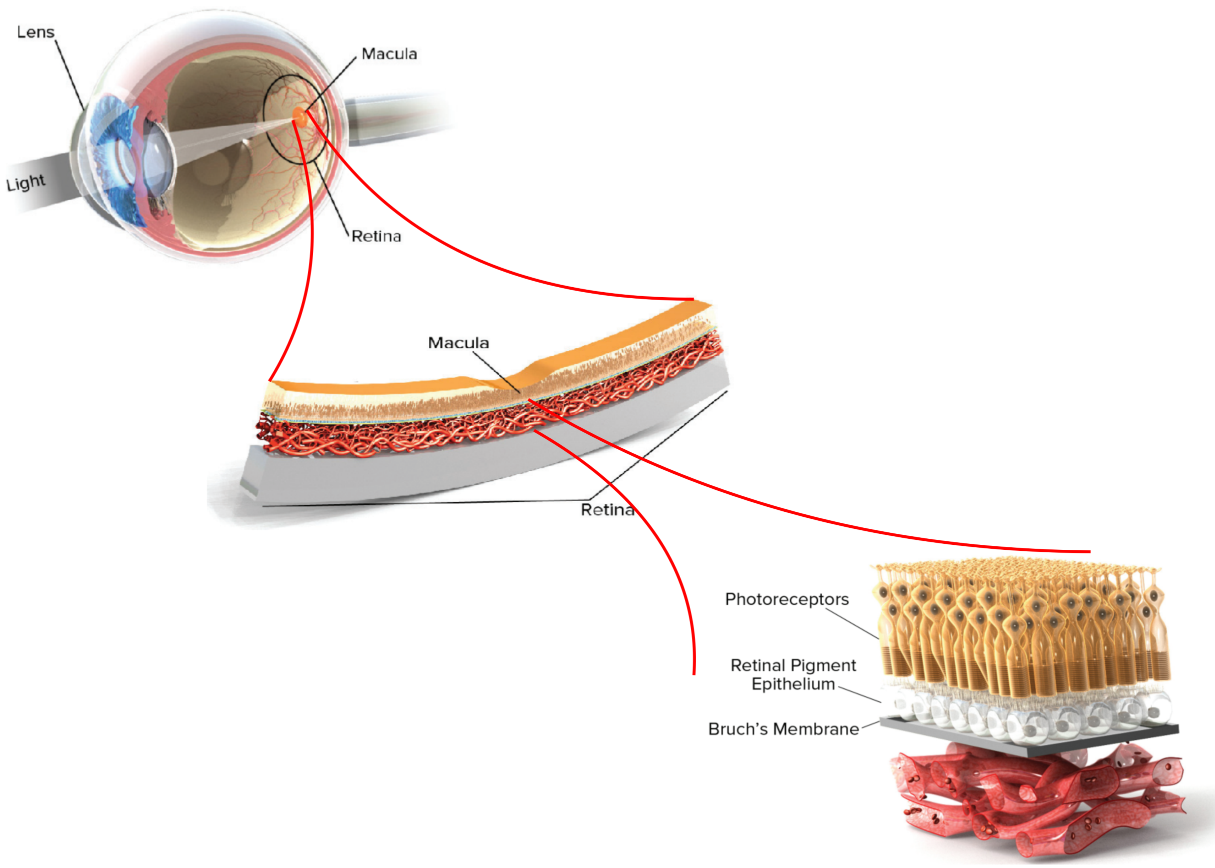

Figure 1.1 (adapted from (1) shows the cross-sectional area of the eye with a focus on the macular to depict the position of the retinal pigment epithelium.

drusen, small yellow deposits that accumulate beneath the retina, are detected in sufficient size and number clinically, causing alterations in the RPE's structural integrity (6). This type of macular degeneration is known as the dry form of macular degeneration (7). The late stage of AMD can be choroidal neovascularization which is the growth of abnormal blood vessels from the choroid underneath the macular towards the outer retina. The occurrence of this is known as the wet form of macular degeneration, it causes fluids to leak below the retina leading to photoreceptor death and severe vision loss(6). However, the vast majority of cases of AMD (90%) remain non-neovascular, for which no treatment exists. Late-stage non-neovascular AMD is termed geographic atrophy and is defined by substantial RPE loss and progressive degeneration of the proximal photoreceptors (6). This condition significantly impacts activities like reading, driving, and recognizing faces(1). Figure 1.2 (adapted from (8)) shows the visual representation of a normal vision in comparison to vision affected by age-related macular degeneration

Figure 1.2 (adapted from (8)) shows the visual representation of a normal vision in comparison to vision affected by age-related macular degeneration. The left side shows two children holding soccer balls, with clear and sharp details. The right side shows the same scene but with a blurred central area, depicting how a person with AMD might see it.

Several studies have established a link between changes in the shape and morphology of retinal pigment epithelium (RPE) cells as early events in age-related macular degeneration (AMD) (7). These morphological alterations in RPE cells are considered significant indicators of the onset and progression of AMD. Researchers have observed that as AMD develops, RPE cells undergo noticeable changes in their structure, which may contribute to the deterioration of visual function. Understanding these early changes is crucial for developing targeted interventions and treatments to slow or prevent the progression of AMD. Although the dynamics behind these changes are yet to be fully understood, numerous attempts have been made to study the shape of RPE cells and structural changes that occur during AMD. For example, a comprehensive study on human eyes utilizing modern computational methods and high-resolution imaging by (9) highlights variations in RPE structures due to age and topographic location. It is noted that RPE cells in the macula maintain a more regular and hexagonal shape but become less pronounced with aging, indicating a gradual disorganization in cell structure. Specifically, the comparative analysis across different age groups in the study showed a general trend of increasing cell size and decreasing density with age. Comparatively, another study (10) carried out on C57BL/6J mice during aging was consistent with the findings in the human model specifying region-specific adaptations of RPE cells within the mice eye and also variations with aging which could be implications for studying diseases like age-related macular degeneration (AMD).

In a study aimed at differentiating RPE cell morphology linked to mouse genotypes and age in (11; 12), it was found that variations in RPE cell morphology significantly correlate with genetic differences and aging. These changes include alterations in cell size, shape, and arrangement, underscoring that RPE morphology evolves with age which could be indicative of AMD. This emphasizes the need to thoroughly understand these structural changes to potentially predict and manage age-related visual disorders.

While many of these studies are presented in 2D in vitro, the complexities of the human organ in vivo means that these models often fail to capture the full details of the RPE cells.

Consequently, they are limited in their ability to explain the structural changes that occur at the onset and during development of AMD.

In 2D, particularly in microscopy flat-mount images, the RPE appears as a tightly packed mosaic of polygonal cells. These cells are predominantly hexagonal ensuring efficient coverage without cell overlap or empty areas. However, the true structure of the RPE becomes clearer in the 3D space. Even though there are relatively few studies detailing the 3D shape of the RPE, recent research has begun to shed light on the complex structure of the cell, moving beyond the limitations of 2D models and providing new insights into the morphology and functional implications in vivo. In two of the most recent studies (13; 14), researchers achieved comprehensive 3D reconstructions of the retinal pigment epithelium (RPE) cells and Corneal Endothelial Cells (CECs), which exhibit similar patterns to the RPE, using human models.

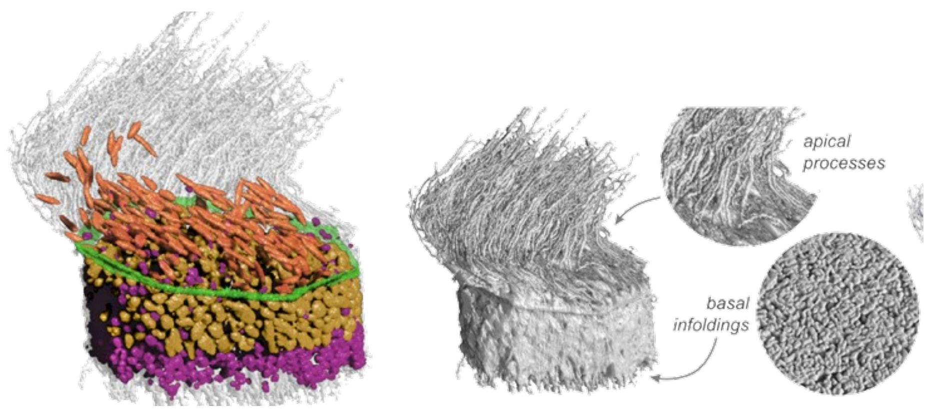

Figure 1.3 (adapted from (13)) shows the reconstruction of RPE cells using a deep learning-assisted volumetric method based on observations from a 21-year-old male donor's post-mortem eye. The image highlights the complexity of the RPE basal surface, including the presence of basal infoldings, which are critical for attachment to the underlying Bruch's membrane and play a vital role in the metabolic exchange necessary for photoreceptor health.

Findings in these studies revealed similar and specialized membrane structures across the

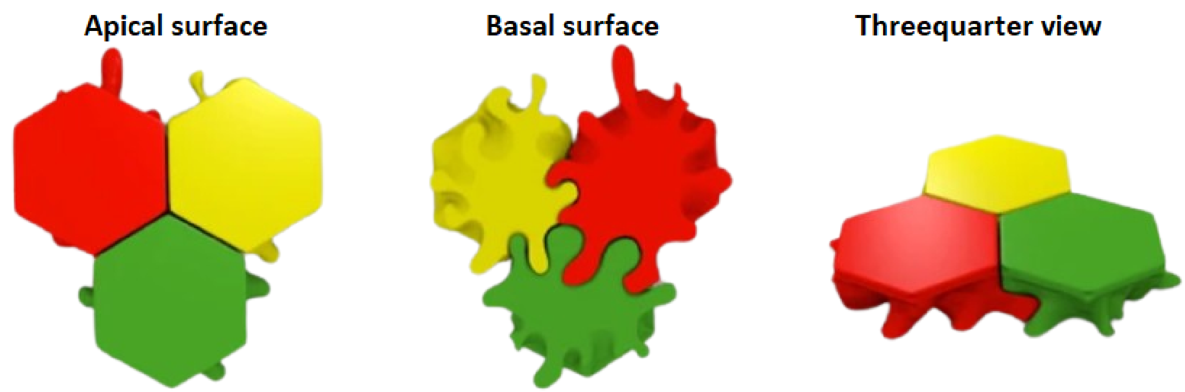

Figure 1.4 (adapted from (14)) showing 3D reconstruction of CECs using computer-aided design and drafting (CADD) software packages based on observations from human models. The image highlights the hexagonal structure of apical surface with tightly joined interdigitating foot processes at the basal surface.

species. The specialized structure, typically presents three different layers which includes apical processes, apico-basal axis and the basal layer. Aside from the observed layers, the studies also revealed the complexity of the basal surface, particularly with the presence of infoldings in the RPE cells as presented by (13) which are critical for the attachment to the underlying bruch's membrane and play a vital role in the metabolic exchange necessary for photoreceptor health. Additionally, the presence of interdigitations in the basal layers of the CECs was presented by (14). These new findings have paved way for more research on the three dimensional studies of the RPE in which computational models can help to reduce the cost of carrying out expensive experimental setups.

1.2 Problem Discussion

Despite the significance of the crucial functions of the retinal pigment epithelium to maintain the well-being of the photoreceptor, understanding its organization and dynamics poses a fundamental challenge. Previous research has detailed the apical-basal polarity of epithelial cells, emphasizing their tight adhesion to neighboring cells at the apical surface, and the formation of lateral cell-cell junction which binds tightly to the basal lamina and provides mechanical stabilization along the apico-basal axis (15). However, the majority of the research focused on the changes that occur in the RPE, especially during AMD, are conducted in 2D, focusing solely on the apical surface of the cell, which limits our understanding of the full cellular dynamics and interactions that occur throughout the entire cell, including the basal and lateral aspects which are essential for comprehensive tissue modeling.

This limitation in research methodologies shows the need for innovative approaches, such as 3D computational modeling, to capture the RPE's full structural and functional complexity. 3D models can offer insights into the interactions across the entire epithelium, potentially revealing novel mechanisms of disease progression. Such advancements could significantly enhance our understanding of RPE-related diseases, leading to improved diagnostic and treatment strategies for conditions like AMD.

1.3 Purpose of the Thesis

To address the gap of study in understanding the structure and dynamics of the RPE in 3D, we embark on a novel journey to develop a comprehensive three-dimensional (3D) computational model of the RPE employing the Cellular Potts Model framework. This model intends to replicate the complex cellular dynamics and architecture of the RPE in vivo, providing insights into the mechanisms driving RPE function, dysfunction, and its interactions.

A particular focus of our study is on exploring and simulating the dynamic expansion and intercalation of the basal footprint of RPE cells. We hypothesize that modulating cellular parameters, such as the target perimeter (in 2D) and surface area (in 3D) coupled with weak cell-to-cell adhesion property not only affects the shape and behavior of individual cells but also facilitates the formation of interdigitations or how well the collective cell structure is preserved.

1.4 Significance of the Study

The significance of this study cannot be overstated, as it addresses critical gaps in the current understanding of the Retinal Pigment Epithelium's (RPE) role in the pathology of Age-related Macular Degeneration (AMD). By employing the innovative approach of 3D modeling using CompuCell3D, this research ventures beyond the limitations of traditional 2D models and in vitro studies, offering a more complex and dynamic exploration of RPE behaviors and interactions within a simulated three-dimensional environment.

CHAPTER 2
METHODS

2.1 The Cellular Potts Model

The Cellular Potts Model (CPM) is an extension of the Potts model, which was originally developed by physicists to simulate magnets. Inheriting concepts from the Potts model, researchers François Graner and James Glazier developed the CPM in the early 1990s to simulate how cells can sort themselves into ordered spatial patterns. The subsequent contributions of Paulien Hogeweg, who extensively applied the CPM, were instrumental in demonstrating its versatility and effectiveness in studying various biological phenomena. Due to Paulien Hogeweg's significant advancements in refining and applying the model across different contexts, the CPM is often referred to as the Glazier-Graner-Hogeweg (GGH) model, acknowledging the foundational work of Graner and Glazier as well as Hogeweg's pivotal role in its popularization (16).

The CPM is a time-discrete Markov process based on a lattice with state space $\mathbb{X}$, in which the transition probabilities are specified with the help of an energy function E (16) . The latter is a function $E : \mathbb{X} \to \mathbb{R}$ that governs the dynamics of the model (17). It is the sum of several terms that control single aspects of the cells' interdependence structure within specific models. The Standard CPM uses two terms which include the surface interaction term between the cell types and also a volume constraint (18).

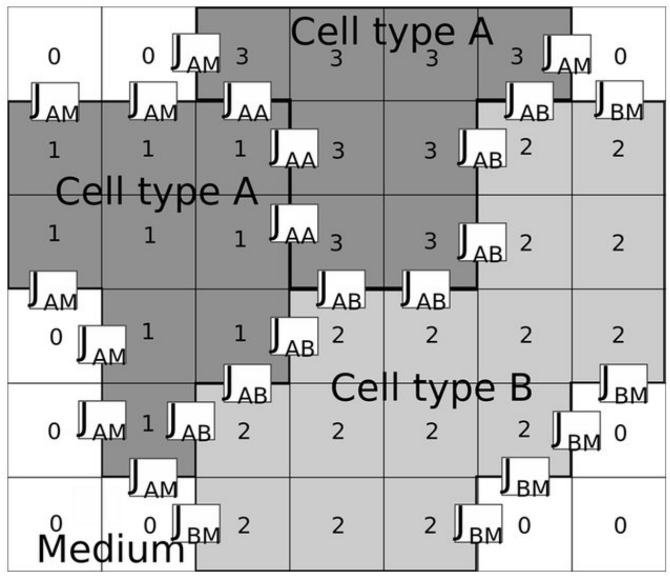

Figure 2.1 Example of a generic configuration of the Cellular Potts Model. The Cells are modeled as sets of square lattice sites. Three cells with indices (”spins”) 1−3 are defined. The index 0 denotes the extracellular matrix (medium). J represents the contact energy between the cell boundaries.

Consider a two-dimensional (2D) space with a variety of cells, each uniquely identified and interacting within a structured lattice. This space, depicted in Figure 2.1, is a visual representation of a CPM, where each site in this discretized area is marked by a value, a numerical identifier from a set that ranges from 0 up to n, where n represents the total number of cells modeled, suggesting the presence of different cells or the medium surrounding them. The lattice, a meticulously arranged grid serves as the stage at which these cells operate. These lattices can be extended into three dimensions to offer a more complex and detailed view of cellular interactions. Interactions between cells, either of the same or different types, are characterized by a concept known as the contact or adhesive energy, denoted by J. This contact energy is a crucial parameter that quantifies the affinity or aversion cells have towards each other, influencing how they adhere to, repel, or otherwise interact with their neighbors within the lattice. Since cells occupy specific spaces within the arranged lattices, they inherently possess an area (or volume in 3D simulations). This spatial characteristic is fundamental to the model, allowing for the simulation of physical constraints and behaviors associated with cellular size and shape. As a result, the total energy governing the standard CPM is the addition of the adhesive term and the area (2D) or volume (in 3D), where:

$$E_s(\sigma) = \sum_{(i,j)} J_{\tau(\sigma_i),\tau(\sigma_j)} \left(1 - \delta(\sigma_i, \sigma_j)\right), \quad \sigma \in \mathbb{X} \tag{2.1}$$

and

$$E_v(\sigma) = \lambda_{\text{volume}} \sum_{\sigma} \left(v(\sigma) - V_{\text{target}}(\sigma)\right)^2, \quad \sigma \in \mathbb{X} \tag{2.2}$$

E_s and E_v above correspond to the energy contributed by surface interaction and the volume constraint, respectively. In addition, the parameter J is the contact or adhesive energy between the cells having σ's as the cell IDs, τ's denote cell types and i and j are labels indicating two neighboring lattice sites respectively. λ_{area} is the strength of the volume constraint, v represents the actual volume and V_{target} is the volume at the target site.

Thus, the total Hamiltonian of a typical CPM is the addition of the adhesive energy between cells and additional terms that may include volume constraints, surface tension, and other cellular properties.

In the described scenario in Figure 2.1, the total energy of the dynamics is:

$$
\begin{aligned}
E &= E_s + E_v && (2.3)\\
&= \sum_{(i,j)} J_{\tau(\sigma_i),\tau(\sigma_j)} \left(1 - \delta(\sigma_i, \sigma_j)\right) + \lambda_{\text{volume}} \sum_{\sigma} \left(v(\sigma) - V_{\text{target}}(\sigma)\right)^2 && (2.4)
\end{aligned}
$$

Depending on the phenomenon under investigation, further parameters, and Hamiltonian terms can be included to fully capture its applicability to real-world biological contexts.

In a CPM simulation, the cell shape dynamics are calculated using a modified Metropolis Monte Carlo algorithm which fundamentally employs stochastic methods to minimize the system's free energy (19). This approach allows the temporal evolution of the cells through probabilistic updates of site identifications or spins. The core principle of the algorithm is to drive the system towards lower energy states, mirroring biological processes where cells reorganize to minimize energy, thereby achieving a more stable configuration. Procedurally, at each discrete time step, t, a lattice site x, belonging to an object interface is randomly selected (source), and proposed to copy its spin $\sigma(x)$ into an arbitrary unlike neighbor x' (target). The change in energy (ΔE) due to this update is accepted with a Metropolis-Boltzmann probability which is given as:

$$
P(\sigma(x) \to \sigma(x'))(t) = \begin{cases} e^{\frac{-\Delta E|_{\sigma(x)\to\sigma(x')}}{T}} & \Delta E|_{\sigma(x)\to\sigma(x')} \geq 0 \\ 1 & \Delta E|_{\sigma(x)\to\sigma(x')} < 0 \end{cases} \qquad (2.5)
$$

ΔE is the net variation of the total energy of the system as a consequence of the spin update.

$$\Delta E|_{\sigma(x)\to\sigma(x')} = E_{\text{after spin}} - E_{\text{before spin}} = E(t) - E(t-1) \tag{2.6}$$

If the energy change ($\Delta E < 0$), the index/spin change is always accepted, whereas if the energy change ($\Delta E \geq 0$), the site index change is allowed with the probability $\exp\left(-\frac{\Delta E}{T}\right)$ where T is a Boltzmann temperature, which does not reflect any conventional thermal temperature, rather correlates to the overall system motility.

In summary, the implementation of the CPM guided by the Metropolis algorithm involves the following steps:

1. **Random Site Selection**: Choose a random site i (source);

2. **Neighbor ID Copy Proposal**: Choose a neighboring lattice site, labeled j, adjacent to site i, and propose to copy the ID (or "spin") from j to i.

3. **Energy Difference Calculation**: Determine the change in the system's Hamiltonian (ΔE) that results from the proposed ID copy. This calculation assesses the energetic consequence of altering the current configuration, encapsulating factors such as adhesion between cells, volume constraints, and other cell-specific properties.

4. **Decision to Accept or Reject the Proposal**:

    - If the new energy is lower, always accept the copy;

- If the new energy is higher, accept the copy with probability $e^{-\frac{\Delta H}{T}}$ (the Boltzmann temperature T determines the likelihood of energetically unfavorable fluctuations).

By repeating these steps iteratively, the CPM simulates the dynamic evolution of cellular structures over time. Each Monte Carlo Step (MCS), comprising a complete cycle through all lattice sites, incrementally advances the simulation, enabling the detailed investigation of tissue development, cellular patterning, and the emergent properties of complex biological systems.

This process might take multiple Monte Carlo Time Steps (MCS) to converge on an outcome that sufficiently resembles any observable behavior that is being modelled and continues until all of the sites on the lattice have attempted such a change (2).

2.2 The Compucell3D (CC3D)

Compucell3D is a robust modelling environment for simulations of biocomplexity problems, mostly at the cellular level (20). By integrating various mathematical models, CC3D serves as a crucial tool for implementing the Cellular Potts Model. It enables users to develop sophisticated simulations more efficiently and rapidly compared to traditional custom coding approaches.

Just like every other computer simulation program, CC3D has an interface for writing configuration files and codes for modifying cell types, properties and simulation parameter and also, a player called CC3D player for carrying out the simulation process.

The default environment where the configuration files and python script is set up and edited is called Twedit, an integrated development environment. The ".cc3d" is an extension for Compucell3D programs and usually contains three (3) sub-files including a XML and two python script files serving as the steppables and its configuration file.

The CC3D Extensible Markup Language (XML) file is a file format and mark up language that allows user to specify details of their cell configurations or attributes such as cell types, properties, interactions, and simulation parameters with ease. It allow for proper configuration of the parameters involved in the Cellular Potts Model. For example, definition of cell volume, contact or adhesion energy within the cells and also, addition of other parameters through the use of a menu called plugin which houses extended properties of cells like growth, mitosis, etc.

The steppable file is mostly a python script or sometimes C++ scripts used for performing operations on cells. Steppables are called at fixed intervals measured in MCS and has three uses which include modifying cell parameters in response to simulation events, to solve PDEs and to load simulation initial conditions or save simulation results.

The software's user-friendly interface simplifies the process of running simulations, enabling users to load their XML files and initiate simulations with a simple click of a button through the CC3D player. The CC3D player is the main simulation program interface with menu including "play", "pause", "forward step", to mention a few. It is used for observing interaction within the cellular model simulations and modelling processes. This approach not only enhances the user experience but also accelerates the setup and execution of complex biological models without excessive writing of codes.

One of the key advantages of utilizing CompuCell3D for biological modeling is its time efficiency. Compared to coding simulations from scratch in languages like C/C++, Java, or Fortran, setting up simulations in CompuCell3D can save significant time and effort. While coding the same simulation in traditional languages could require at least 1000 lines of code, CompuCell3D streamlines the process with its XML-based configuration. Additionally, the software allows for easy modification of simulation parameters and logic without the need for recompilation. Users can adjust settings in the XML file or Python scripts and rerun simulations seamlessly, eliminating the time-consuming recompilation processes typically associated with traditional coding approaches.

Furthermore, CC3D benefits from active development, maintenance, and support within a dedicated community. With regular releases, comprehensive documentation, and user forums, CompuCell3D provides a dynamic platform for biological modeling. The software's versatility extends to a wide range of applications in biological research, including cell behavior studies, tumor growth and invasion modeling, and developmental biology investigations. By simulating complex biological processes such as cell sorting, chemotaxis, proliferation, differentiation, tumor progression, and tissue development, researchers can gain valuable insights into the underlying mechanisms driving these phenomena. Overall, CompuCell3D stands as a valuable tool for studying biological systems, offering researchers a flexible, efficient, and well-supported platform for conducting sophisticated simulations and analyses.

2.3 Model Initialization

The introduced computational model simulates the complex structure and interactions within the Retinal Pigment Epithelium (RPE) cell. This model, built using the CC3D platform, focuses on the three main forces regulating cell surface mechanics - adhesion-driven tension, cortical tension and pressure within the CPM framework. The model development occurs in two stages. The first stage is a simple 2D representation of a single RPE cell layer representing, the Basal cell. This simplified 2D setup serves as a foundation for understanding the fundamental cellular behaviors and interactions that contribute to basal surface expansion and cell interdigitation. Next, the model progresses to a 3D structure consisting of three (3) interconnected regions of the RPE cell which include apical, lateral, and basal surfaces, all lying on the Extracellular Matrix (ECM).

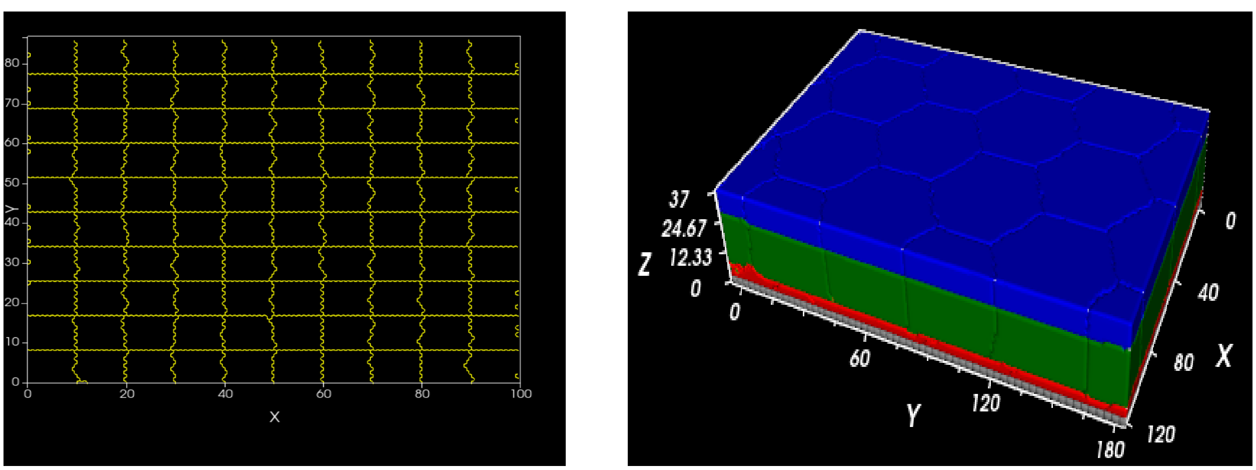

(a) (b)

Figure 2.2 (a) 2D initial cell setup in CC3D with cell size 10 on a 100×100 pixel. Hexagonal cell lattices were set for the cells, however, the initial cell layout always begin with the square lattices before transforming to the target (hexagonal) lattice. (b) 3D initial cell layout showcasing the apical (blue), lateral (green), basal (red) and the ECM (ash) on $120 \times 180 \times 37$ pixel.

The initial configuration of the cells is shown in Figure 2.2 which correspond to the 2D and 3D models respectively.

2.3.1 2D Model Governing Equation

In the 2D case, based on the configuration of the cells involving cell contacts with themselves, an area which keeps them from collapsing and the fact they each have a boundary separation, three (3) basic parameters were selected which include the cell area, cell perimeter, and contact energy or adhesion parameter. As a result, the governing energy equation within the Cellular Potts Model is given as:

$$\begin{aligned} E &= E_c + E_a + E_p \\ &= \sum_{(i,j)} J_{\tau(\sigma_i),\tau(\sigma_j)} \left(1 - \delta(\sigma_i, \sigma_j)\right) + \lambda_a \sum_{\sigma} \left(a(\sigma) - A_{\text{target}}(\sigma)\right)^2 \\ &+ \lambda_p \sum_{\sigma} \left(p(\sigma) - P_{\text{target}}(\sigma)\right)^2 \end{aligned} \tag{2.7}$$

Where E represents the total energy of the system which is a sum of contact energy E_c, area elasticity energy E_a, and perimeter elasticity energy E_p. The contact energy E_c is calculated based on the adhesion parameter $J_{\tau(\sigma_i),\tau(\sigma_j)}$ and the Kronecker delta function $\delta(\sigma_i, \sigma_j)$, which differentiates whether cells are identical or different. The area elasticity energy E_a penalizes deviations from a cell's target area $A_{\text{target}}(\sigma)$, promoting volume consistency, while the perimeter elasticity energy E_p manages the cell's perimeter by penalizing deviations from a target perimeter $P_{\text{target}}(\sigma)$, helping to maintain cell shape.

The parameters λ_a and λ_p are coefficients for the elasticity of area and perimeter, respectively, which are also referred to as Lagrange multiplier, dictating the strength of penalties for deviations from target values. $J_{\tau(\sigma_i),\tau(\sigma_j)}$ serves as the adhesion coefficient between different types of cells, influencing how strongly they adhere or repel each other. Negative values of J signify attraction while positive values denotes repulsion. $a(\sigma)$ and $p(\sigma)$ represents the actual area and perimeter, respectively. $A_{\text{target}}(\sigma)$ and $P_{\text{target}}(\sigma)$ are the target area and perimeters, respectively.

We configured the cells to occupy an area of 100×100 pixels on a hexagonal lattice within the Compucell3D platform. The hexagonal lattice was chosen for this simulation because it better reflects the natural packing of RPE cells, which are mostly hexagonal in vivo.

The periodic boundary condition was set at both x and y boundaries allowing the cells to interact freely across the lattice, effectively eliminating edge effects or artificial edges and allowing for a more naturalistic representation of RPE cellular behaviours and interactions occurring as a continuous sheet in vivo. By periodic boundary condition, we mean a cell moving off one edge of the lattice reappears on the opposite edge, ensuring continuous and unrestricted movement.

By default, in Compucell3D, the cell layout always starts as a square-shaped cell lattice. As such, the length of the cells is set at 10 with each area summing up to 100. Mathematically, based on the hexagonal lattice type applied during the simulation and the motive of obtaining a hexagonal shape, the target area was set at approximately 93.53 representing the actual area of the cells that can be obtained within the initial target area of 100 for each square lattice layout implying that each hexagonal side is 6 using the formula for calculating the area of a hexagon,

$$A = \frac{3\sqrt{3}}{2} \cdot l^2 \tag{2.8}$$

where A is the area and l represents each side of the hexagon. However, this did not take effect since the periodic boundary conditions are applied.

Based on the observed simulation preliminary results, the neighbor order was set at 1. An increase in the neighbor order was observed to cause the cells to have a prolong time before reaching equilibrium but resulting into the same outcome. Also, the temperature, T, as in the context of the Metropolis Algorithm was set at 15.0 for most of the simulation. The temperature parameter is not a direct representation of physical temperature but is analogous to it in the sense that it controls the level of intrinsic fluctuation or motility of the cell membrane within the simulation.

2.3.2 3D Model Governing Equation

Building upon the 2D model, the 3D lattice adopts dimensions of 120 x 180 x 40 pixels. Cells are arranged on a hexagonal lattice, reflecting the natural packing of RPE cells. As identified by existing literature on RPE morphology, the model incorporates three distinct cell layers stacked vertically: apical (top), lateral (middle), and basal (bottom) resting on an extracellular matrix (ECM). Periodic boundary condition was also considered for both x and y sides to allow for unrestricted shape of the cell.

Similar to the 2D case, three distinctive physical properties of the cell surface mechanics including volume, contact energy or adhesion parameter, and surface area are considered within the Compucell3D simulation environment. As a result, the governing energy equation of the system in 3D is given as:

$$
\begin{aligned}
E &= E_c + E_v + E_s \\
&= \sum_{(i,j)} J_{\tau(\sigma_i),\tau(\sigma_j)} \left(1 - \delta(\sigma_i, \sigma_j)\right) + \lambda_v \sum_{\sigma} \left(v(\sigma) - V_{\text{target}}(\sigma)\right)^2 \\
&+ \lambda_s \sum_{\sigma} \left(s(\sigma) - S_{\text{target}}(\sigma)\right)^2
\end{aligned}
\tag{2.9}
$$

The neighbour order is set to be ≥ 2, making spin copy attempt possible to nearest and second-nearest neighbors with at least a total of eight neighbours for each lattice site and the temperature parameter T at 15.0 is maintained all through the simulation.

Throughout the simulation, the following assumptions were made in the modeling approach, including those related to cell behavior, interactions, and the environment includes:

- Cells are assumed to maintain a hexagonal shape in both 2D and 3D representations.
- The ECM is considered static and uniform throughout the simulation.
- **Homogeneity of Cell Properties**: It is assumed that all cells within a given layer (apical, lateral, basal) exhibit uniform properties such as area or volume, perimeter, and adhesion parameters.

Parameter	Value		Description
	2D	**3D**	
Cell type	Basal Cell	Apical, Lateral, Basal Cell & ECM	The 2D model features a single layer of Basal cells. In contrast, the 3D model includes multiple layers comprising Apical, Lateral, and Basal cells, along with an Extracellular Matrix (ECM).
Lattice dimensions	100x100	120 x 180 x 40	Cartesian lattice size and 3D dimension for the cell layout
a or v	93.53	calculated based on cell dimension defined in the python script	a represents the 2D actual cell area while v represents the cell volume in 3D
λ_a, λ_v, λ_p, λ_s	2.0	2.0	λ is a Lagrange multiplier determining the strength of the parameters denoted in the subscript where a is the area, v - volume, p - perimeter and s - surface area
J	Weak adhesion to favour complex structures and allow for intercalation within the basal layer	Varies between cell layers and cell types	Cell-Cell contact adhesion energy defined with the assumption of strong bonds between the apical and lateral cell layer, a bit relaxed adhesion energy and weak adhesion energy between the lateral and basal
T	15.0	15.0	Fluctuation parameter. Higher values make it more likely for spin flips to occur.

Table 2.1 Initial simulation parameter within the 2D and 3D cell model setup

- **Simplified Adhesion Parameters**: The complexity of cell adhesion mechanisms is reduced to a single adhesion parameter in both 2D and 3D simulations, simplifying the diverse range of molecular interactions into a more manageable form.

- **Periodic Boundary Conditions**: Cells in both 2D and 3D models utilize periodic boundary conditions, allowing them to move freely across the lattice and interact with cells on opposite edges. This eliminates edge effects and simulates continuous interaction.

- The model focuses on physical properties related to cell surface mechanics, neglecting other biological processes or cellular components for simplicity.

CHAPTER 3

2D SIMULATION OF RPE BASAL CELL MORPHOLOGY USING CELLUAR POTTS MODEL

3.1 Quantitative Analysis of Morphological Changes and Interdigitation in RPE Cells

This section presents the detailed quantitative analysis of morphological changes in the retinal pigment epithelium (RPE) basal cells simulated in a two-dimensional environment using the Cellular Potts Model (CPM). The main focus lies on understanding how cell morphology evolves and interdigitates under varied simulation conditions.

A two dimensional (2D) cellular potts model (CPM) was used to set up a total of a hundred (100) squared cells on a 100×100 pixel grid to initiate the simulation. A hexagonal cell lattice was applied through the compucell3D software to encourage the cells to evolve from their initial square form into hexagonal shapes and mimic the biological behaviour of the RPE cell more closely. Figure 3.1 shows the transition of these cells from the initial square layout to hexagonal shape.

To accurately simulate interdigitation formation, we began by searching for a control parameter that influences interactions among cells through random variation of the adhesion, area and perimeter. Ultimately, we identified the perimeter, P, as the critical control parameter corroborating findings from (21) on confluence systems.

We concentrate on investigating the effect of increasing perimeter on the cell shapes. At the simulation's onset, we found a minimum perimeter value, P_{min} of the system which

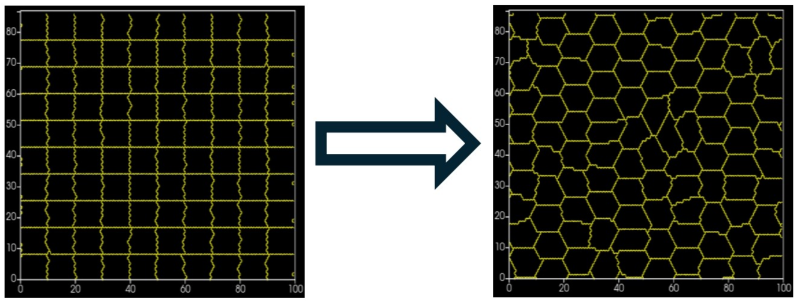

Figure 3.1 Transition of cells from the initial square to hexagonal shapes. (Left) Initial configuration where each cell is shaped as a square, neatly arranged on a 100x100 pixel grid. (right) at 250mcs depicts the state of the simulation where the cells have transformed into irregular hexagonal shapes depicting a more biologically realistic model, which optimizes packing and reduces boundary energy.

lies between $44.0 \leq P_{avg} \leq 45.0$ due to the geometric constraints and an initial average perimeter, $P_{avg} \approx 48.39$. Starting with different target perimeter P_0 values, we observed two (2) distinct phases and a transition phase based on the perimeter settings.

Figure 3.2 (a) shows the temporal dynamics of the system in the first phase. For small values of target perimeter, P_0 such that $P_0 < P_{min}$, the initial average perimeter, P_{avg} of the system continually minimizes to reach an equilibrium point at P_{min}. In this phase, any selected target perimeter P_0 is classified as low target perimeter in which cells attempt to adjust their pixels to facilitate the retention of the hexagonal shapes.

Above this point, we found a transition point which lies at approximately values $\geq P_{avg}$ where selected target perimeter values overcame the geometric constraint within the cells and shift away from their attempt in becoming a hexagonal shape to a point where some levels of interdigitation is observed within the cell−cell boundaries. We labelled this phase as the high target perimeter P_0 phase. A consistent increase in the P_0 within this phase gradually produces complex structures indicating interdigitation between the cells.

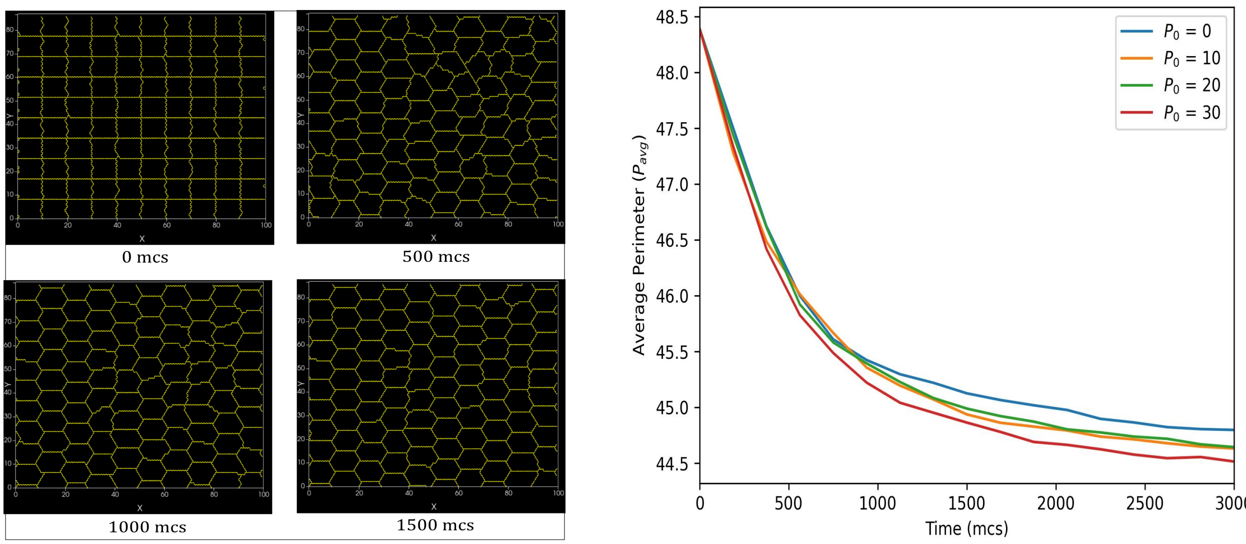

(a) (b)

Figure 3.2 (a) Dynamics of the cell shapes in the low P_0 phase over time. Starting from an initial square configuration (0 mcs), cells evolve through a series of Monte Carlo steps towards more biologically realistic hexagonal shapes. At 1500mcs, most cells have adopted a near uniform hexagonal shape. (b) The graph displays the dynamics of the average perimeter of cells simulation over time, measured in Monte Carlo Steps (MCS) within the low target perimeter P_0 phase. It tracks the changes in average perimeter under different target perimeter settings (P_0), specifically for P_0 values of 0, 10, 20, and 30 indicating the minimization from the initial P_{avg} to P_{min}

The transition phase which lies between ($P_{min} < P_0 < P_{avg}$) is observed to produce erratic behavior where cells' average perimeter do not settle to a certain equilibrium point but haphazardly range between values slightly lower and above the initial P_{avg}. Full interpretation of this phase isn't very well understood, however, the visual results of the simulation depict a combination of straight edges and slight interdigitation within the cells. Figure 3.4 presents a phase diagram summarizing the effect of increasing perimeter value at 2000mcs where the target perimeter value $P_0 = 48.39$ indicating a point within the transition phase where the cell do not settle to an equilibrium point (hexagonal shape or interdigitated boundaries).

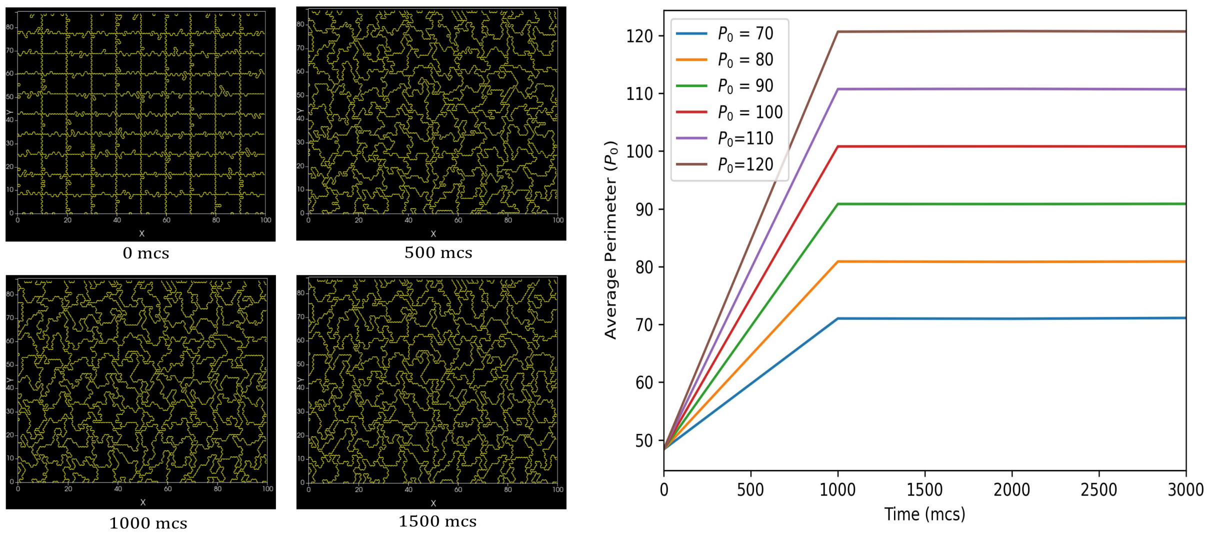

(a) (b)

Figure 3.3 (a) Dynamics of the cell shapes in the high P_0 phase over time. Starting from an initial square configuration (0 mcs), cells evolve through a series of Monte Carlo steps towards a complex irregular shapes with protuding and intruding boundaries representing interdigitation within the cells (b) The graph displays the dynamics of the average perimeter of cells simulation over time, measured in Monte Carlo steps (mcs) within the high target perimeter P_0 phase. It tracks the changes in average perimeter under different target perimeter settings (P_0), specifically for $P_0 > P_{avg}$, indicating that the perimeter constraint is satisfied.

3.2 Adhesion Dynamics

A crucial aspect of our study involves the interplay of both adhesion energies and perimeter constraints on cell morphology and interactions. Our initial hypothesis suggested that interdigitation could be achieved using weak negative adhesion (attractive force) and perimeter constraints. However, our simulation outcomes shows otherwise demonstrating that the dynamics of the cell are consistent across both the positive and negative values. This result aligns with the previous research findings by (22), which indicate that adhesion energies and target perimeter have a one-to-one mapping relationship.

As a result of the findings in (22), we proceeded to investigate if increasing or decreasing the target perimeter, P_0, makes up for the value of the adhesion energy. This is due to the one-to-one mapping relationship between J and P_0 suggesting that modifications in one parameter should reflect alterations in the other. For example, if P_0 is decreased, theoretically decreasing the adhesion energy should reflect the same similar dynamics. Conversely, if P_0 is increased, increasing the the target perimeter could counterbalance this effect such that the original cell behaviour and interactions is preserved. Although, we could not account for the scaling factor discussed in (22), it is evident that there is a one-to-one mapping relationship between both adhesion energy, J and target perimeter, P_0 and produces same cellular dynamics irrespective of the sign of J. Figure 3.4 below shows the phase plot of P_0 versus J depicting similar cellular dynamics between negative and positive J value in response to increasing target perimeter, P_0

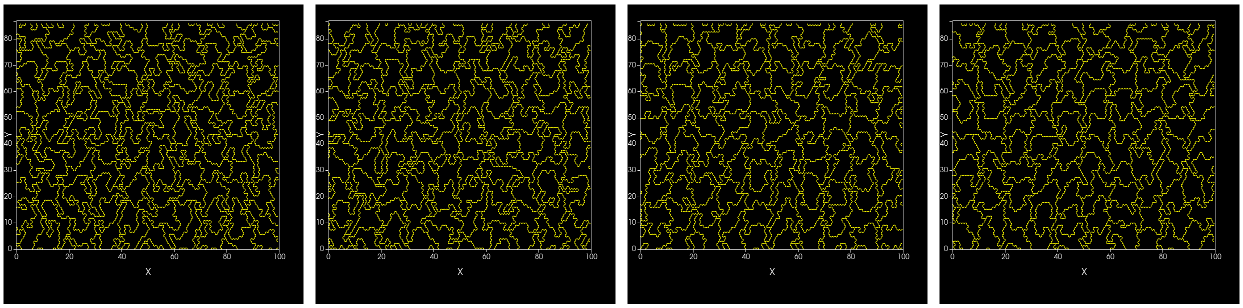

(a) $J = -20, \quad P_0 = 80$ (b) $J = -10, \quad P_0 = 80$ (c) $J = 10, \quad P_0 = 80$ (d) $J = 20, \quad P_0 = 80$

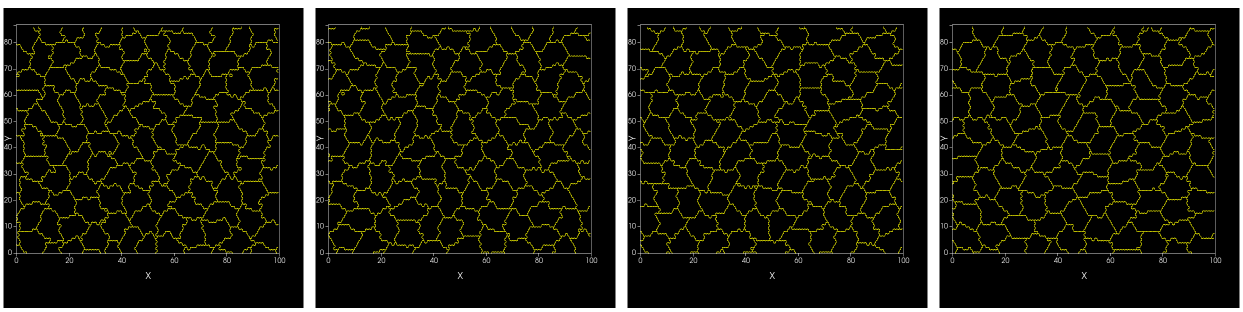

(e) $J = -20, \quad P_0 = 48$ (f) $J = -10, \quad P_0 = 48$ (g) $J = 10, \quad P_0 = 48$ (h) $J = 20, \quad P_0 = 48$

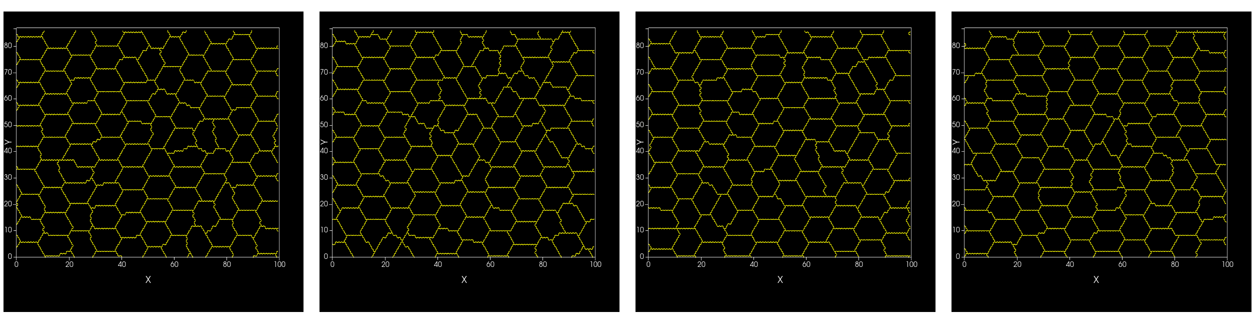

(i) $J = -20, \quad P_0 = 10$ (j) $J = -10, \quad P_0 = 10$ (k) $J = 10, \quad P_0 = 10$ (l) $J = 20, \quad P_0 = 10$

Figure 3.4 Phase diagram showing the effects of increasing target perimeters (P_0) vs varying contact energies (J) on cell morphology within the Cellular Potts Model framework. A one-to-one mapping between adhesion energy J and target perimeter P_0 presenting that varying the adhesion energy between negative values and positive values results into same dynamics.

CHAPTER 4
SIMULATION OF THE RPE CELL IN 3D

4.1 Dynamics of Interdigitation and Infolding the Basal Cells in 3D

Building on the findings from the 2D simulations discussed in Chapter 3 and the fact that recent research on the biophysical nature of cells posits that cell shapes are a consequence of the cell surface mechanics, we decided to extend the investigation into 3D, employing similar computational method as in the 2D morphological structure (22). For the 3D computational modelling, we considered the surface area, volume and adhesion energy as described in the governing equation based on the CPM framework in chapter 2.

Our conceptual model is designed to align closely with the recent findings presented by Lindell et. al (13) on RPE cells and the work by He, Zhiguo, et al. (14) on corneal endothelial cells which is similar to the structure of RPEs. Their work explicitly described three layers of the cells along the apical to basal axis and as such, we developed a three layers of the RPE cell labelled apical, lateral and basal cell and an extra fourth layer, the extracellular matrix which serves as a foundation supporting these cells. In addition, both research works specifically stated a special infolding or interdigitation found in the regions of the basal cells. While our main focus is to investigate the formation of interdigitation or interlocking and infoldings structure in the basal cell, there is need to include the other cell layers to replicate the 3D cellular environment more accurately.

As previously discussed, the initial configurations of the 3D models started with cuboidal cells aligned on a $120 \times 180 \times 40$ pixel grid. The compartmental layers include the apical, lateral, basal and an extracellular substrate on which these cells are resting. Unlike in the 2D set up where the cells start as squares, the 3D cells initial layout is in hexagonal packing, reflecting a complex spatial organization observed in natural cellular environments.

Just as in the 2D process, the interdigitation process was obtained through the surface area constraint and adhesion energy. However, the process is more complex and the adhesion dynamics differs from what it was in the two dimensional structure. The contact energy, J between the cell layers play crucial role in the morphology of the cell structure and as such they are setup distinctively across the cell boundaries and cell types. Since there are a total of four cell compartments with description from in vivo experiments stating that the cells at the apical have tight end-to-end junctions, within our simulation, the adhesion and surface energies within the model are adjusted such that the apical cells exhibit a tight surface constraints that minimizes ripples, theoretically represented by lower contact energy and reduced surface area compared to the other cells. To prevent mixing of the cells within this layer, the repulsive contact forces were applied which is synonymous to positive J values theoretically, ensuring that the cells maintain their integrity and spatial separation within the simulation environment.

The contact energy between the compartment layers is carefully calibrated to prevent the cells from mixing by setting the interaction energies in a way that discourages cells from migrating across their designated compartments. For example, basal cells are prevented from moving into the lateral membrane area during the simulation and likewise for the other cell types. We investigated the interplay of J (contact energy) and the target surface area, S on the cellular behaviour and formation of interdigitation and infoldings within the basal cell. Preliminary results revealed that the contact energy between lateral-basal and basal-ECM is an important factor to consider during the simulation coupled with the increase surface area of the cells. While the surface area for the lateral and basal cell types was correctly adjusted to enhance formation of complex structures, four modes of adhesion energy were explored to assess their impact on the cellular configurations and interdigitation processes. The four modes considered for this process are summarized in the table below.

Modes	**Lateral-Basal**	**Basal-Basal**	**Basal-ECM**
I	$J > 0$	$J > 0$	$J > 0$
II	$J < 0$	$J < 0$	$J < 0$
III	$J > 0$	$J < 0$	$J > 0$
IV	$J < 0$	$J > 0$	$J < 0$

Table 4.1 Adhesion energy settings for different interactions

The adhesion energy is structured such that the J values between Lateral-Basal and Basal-ECM interactions are aligned in the same direction, either both positive or both negative. Additionally, the Basal-Basal interactions are set to consider both negative and positive J values, which may sometimes alternate with the sign of adhesion of the other cell layers.

As detailed in Table 4.1, the adhesion energy interactions for modes I, II, and III are structured with specific J values alignments. We began setting up as shown in Table 4.1, adhesion energy interaction in modes 1, 2 and 3 coupled with an increase in surface area.

Considering the adhesion settings in mode 1, where the adhesion interaction is set at positive for all J values, we observed that the cells tend to exhibit a behaviour where the cells are discouraged from approaching each other, leading to lack of interdigitation but presence of infoldings similar to the experimental result in (13). Figure 4.1 below shows the simulation result of the cells in mode 1.

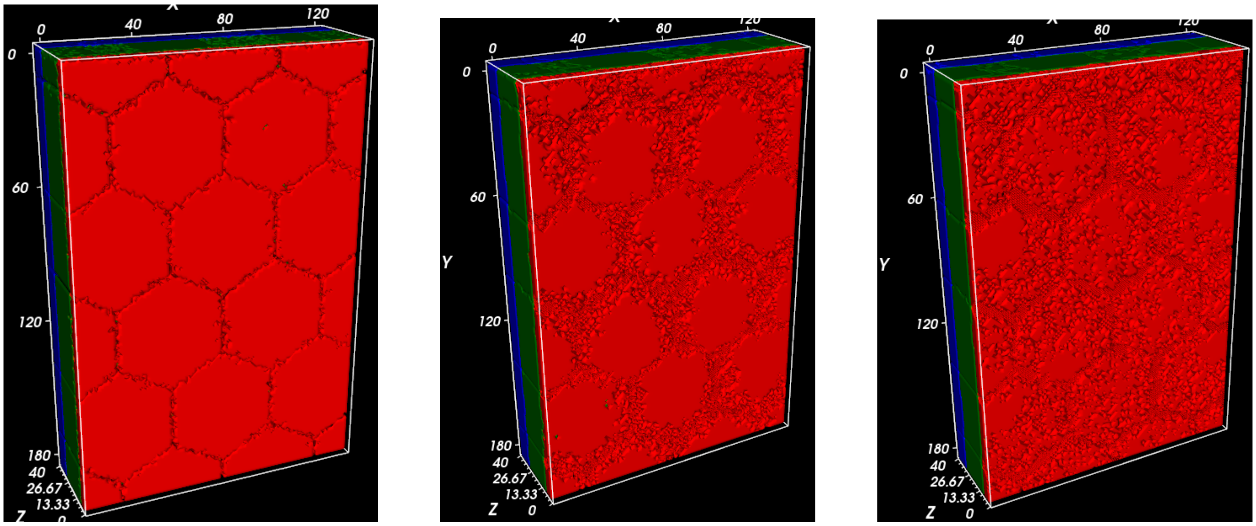

(a) 0mcs (b) 20mcs (c) 100mcs

Figure 4.1 Adhesion parameter settings in mode 1 with $J_{Lateral-Basal} = 10.0$, $J_{Basal-Basal} = 5.0$, $J_{Basal-ECM} = 10.0$. At 0mcs, the cells are at their original hexagonal structure with distinct and separated boundaries. As time progresses, the boundaries between the cells begin to blur out and eventually lose the distinct hexagonal boundaries indicating that the repulsive forces within the basal cells are mostly countered by other constraints thereby resulting into infoldings in the basal cell.

In mode 2, we considered all negative J values between the basal-basal cell and also in their interactions with the lateral cell and ECM to see if the attractive forces coupled with the surface area constraint will produce the desired interdigitation. While some wiggling in the cell boundaries was observed over time as shown in figure 4.2, the cells were unable to go beyond the boundary wigglings. The same outcome is observed in mode 3 where the negative J value is retained for basal-basal cell while the lateral-basal and basal-ECM layers are configured with positive values. However, a slight difference involving breakage from the cell boundaries when simulated over a longer time as displayed in figure 4.3, which might be due to stress which exceed the structural limits.

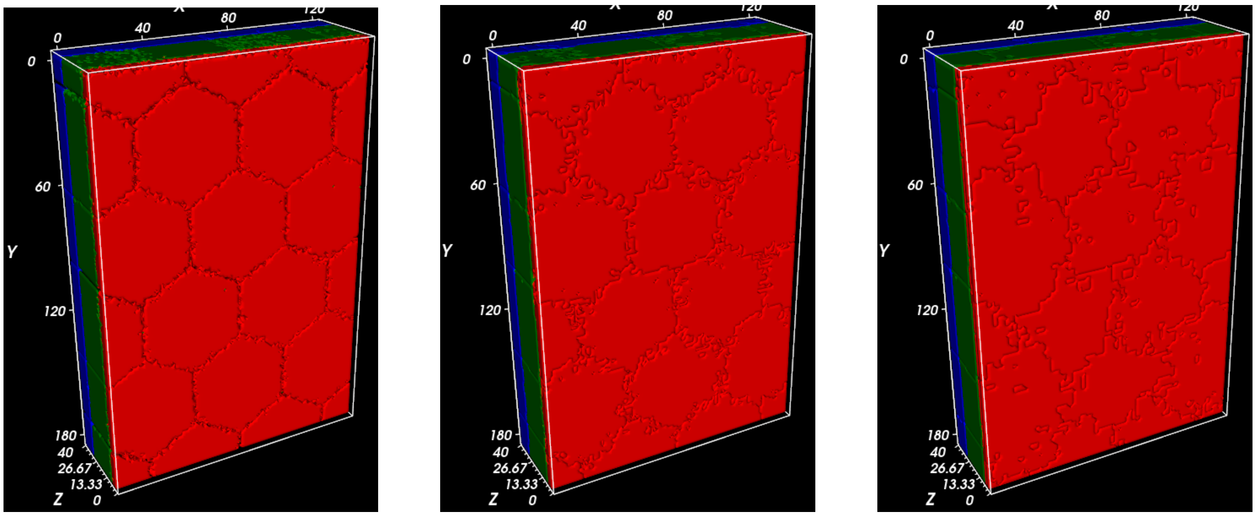

(a) 0mcs (b) 20mcs (c) 300mcs

Figure 4.2 Adhesion parameter settings in mode 2 configured with $J_{Lateral-Basal} = -10.0$, $J_{Basal-Basal} = -5.0$, $J_{Basal-ECM} = -10.0$. At 0mcs, the cells are at their original hexagonal structure with distinct and separated boundaries. The cell boundaries begin to wiggle over time showing some form of interlockings only at the boundary.

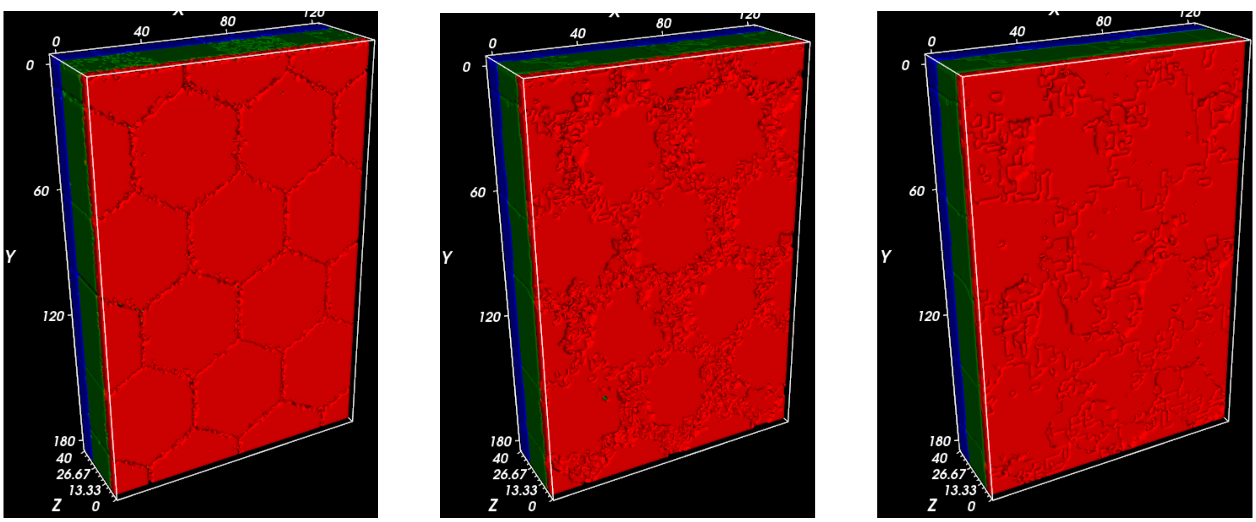

(a) 0mcs (b) 20mcs (c) 300mcs

Figure 4.3 Adhesion parameter settings in mode 3 configured with $J_{Lateral-Basal} = 10.0$, $J_{Basal-Basal} = -5.0$, $J_{Basal-ECM} = 10.0$. At 0mcs, the cells are at their original hexagonal structure with distinct and separated boundaries. The cell boundaries begin to wiggle over time showing some form of interlockings only at the boundary which later breaks off

Finally, we configured our model using the parameters defined in model 4 where the interaction between the basal-basal cells are set to repel each other while an attractive force is set between their interactions with both the Lateral cell and the ECM, respectively.

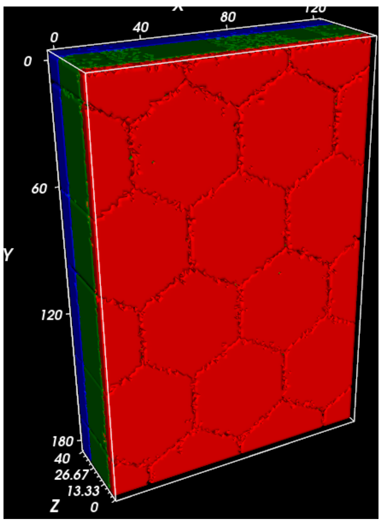

(a) 0mcs

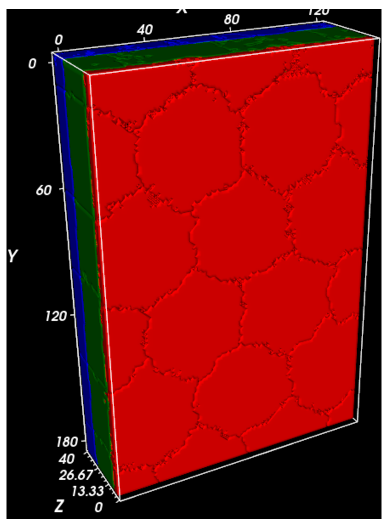

(b) 50mcs

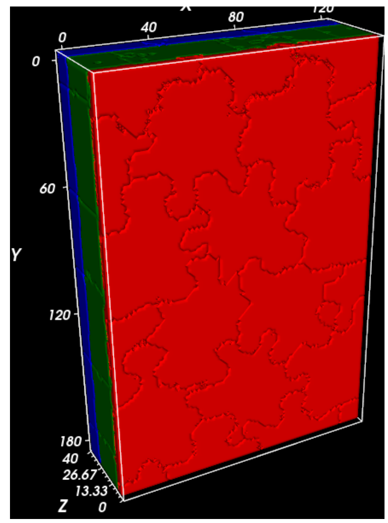

(c) 150mcs

Figure 4.4 Adhesion parameter settings in mode 4 configured with $J_{Lateral-Basal} = -10.0$, $J_{Basal-Basal} = 5.0$, $J_{Basal-ECM} = -10.0$. At 0mcs, the cells are at their original hexagonal structure with distinct and separated boundaries. Thereafter a progression into fluid-like with boundary wigglings which later developed into interlockings or interdigitations within the basal cells as seen at 100mcs

As shown in figure 4.4, with this confirguration, the cells are able to overcome the geometric constraint and form interdigitation similar to the result in of the single basal cell of CECs described in (14).

CHAPTER 5
DISCUSSION AND CONCLUSION

With the use of biophysical parameters of the CSM model under the CPM framework and computer simulation, we have been able to gain an insight into the formation of interdigitation within the basal cells of the retinal pigment epithelium (RPE). We began our model initialization with a 2D simulation of cells under hexagonal lattice constraint to replicate the closely packed, orderly arrangement typical of epithelial tissues. This setup was chosen to model the natural geometric configuration of cells, particularly in the RPE. Thereafter, we employed some of the insights gained through the 2D simulation into the 3D simulation to investigate the formation of interdigitation and infolding surfaces in these cells when they are in their natural form which involves layers of compartmental cells which might contribute to their morphology. Our initial hypothesis propose that an increase in surface area where cells are able to overcome their geometric constraints coupled with a weak adhesion are responsible for these observed structures. This hypothesis is grounded in the notion that when cells have more surface area to contact their neighbors but are only weakly adhesive, they may extend and interlock with each other to maximize stability and cohesion within the tissue structure.

In the 2D simulation, the cells are setup in confluence with periodic boundary conditions which allow each cell to retain the same area and interact continuously across the boundaries of the simulation area. As a result of this, the dynamics of the cells presented in this study are independent of the area of the cells. Our simulation results show that dynamics of the cells are dependent on the perimeter which serves as the control parameter. We found two different regions of the dynamics and a transition point which includes a low target perimeter regions where cells are unable to overcome their geometric constraints thereby retaining their hexagonal structure and also, a high target perimeter region, usually greater than the average perimeter of the cells in which interdigitation occurs. The transition phase lies between both the low P_0 and high P_0 region where some forms of instabilities occur - cells fluctuating between forming hexagonal structure with straight edges and wiggling edges. We observed that an increased surface area which maximizes the average perimeter of the total system beyond the minimum perimeter P_{min} produces the wiggling boundaries and eventually leads to interdigitation. Building on our earlier findings and to refine our initial hypothesis, our observations indicate that within the CPM framework, while the perimeter acts as a control parameter, a decrease in the adhesion strength leads to similar dynamics as increasing the target perimeter, P_0. In addition, there is no difference between using a positive or negative J value.

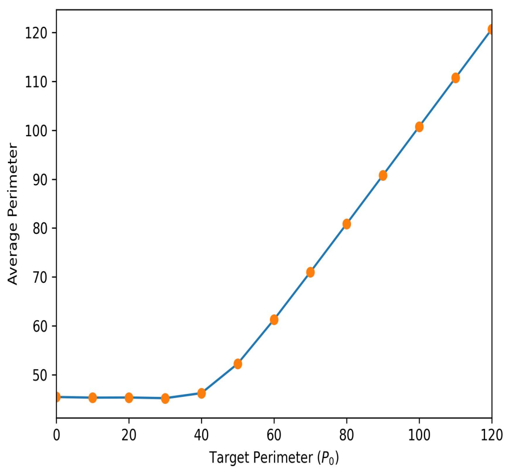

(a)

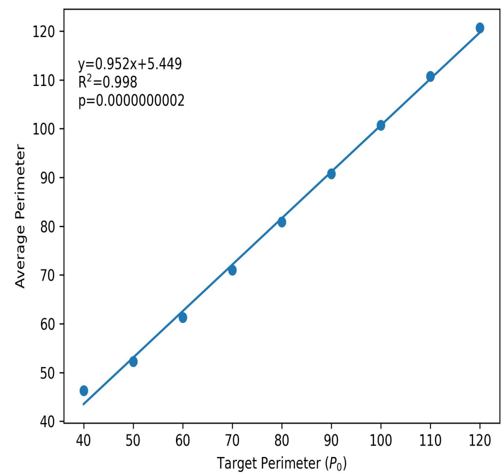

(b)

Figure 5.1 displays two key relationships of the 2D simulations, showcasing how variations in the target perimeter, P_0 influences cell morphology. (a) is a trendline summarizing the average perimeters of the cells against P_0. P_0values below 48.39 shows converges at the minimum average perimeter of the system, thereby cells retaining their hexagonal cells. P_0 values greater than this point are able to cause the average perimeter to increase, depicting an increased wiggle behaviour in cell boundaries and consequent interdigitation (b) presents a correlation analysis for target perimeters above the threshold, highlighting a linear increase in average cell perimeter as P_0 increases.

Figure 5.1 (a) summarizes the dynamics of the system in the 2D simulation environment, highlighting the effect of increasing target perimeter, P_0 on the cell morphology. For target parameter at 0 - 40 which represents the lower P_0 regions, it is noticed that the cells average perimeter is constant thereby retaining their hexagonal shapes with straight edges. Further increase in the P_0 parameter at values greater than P_{min} or the initial saturation level causes the cells average perimeters to increase resulting into cell boundary wiggles and consequent interdigitation. Relationship between the average perimeter of the system at high P_0 region shows a linear correlation plot with positive slope indicating that as P_0 is increased beyond the minimum geometric constraint, the cells are able to expand their boundaries accordingly as shown in figure 5.1 (b).

We extended our work to explore the three-dimensional (3D) model, applying insights gained from the 2D simulations to a more complex, 3D context. A three (3) layer of compartmental cells including apical, lateral and basal with an additional extracellular matrix (ECM), which serves as a foundational support. We hypothesize that adhesion strength between the layers of the cells decreases from the apical to the ECM with the apical exhibiting tight surface constraint that minimizes ripple, cells in the lateral region showing noticeable effects of ripples. The basal layer, with the weakest adhesion strength among the three, exhibits pronounced tendencies for ripple effects and interdigitation. Unlike in the 2D model, the 3D model revealed that while an increase in the surface area of the cells are responsible for promoting interdigitation, the adhesion interactions within the layers of the cells also play a critical role in determining the extent and nature of these interdigitations, infoldings and other structural changes Figure 5.2 shows the XY plane of the layers of the cells after 150mcs capturing the moment when interdigitation of the basal cells have occurred and revealing the wiggling surface of the lateral cell and the tight end-to-end hexagonal packing of the apical cell.

The adhesion interaction within the layers of the basal cell and the cells directly above and below, coupled with their interplay with increased surface area, form the major pivot point for interdigitation within the basal cells.

In summary, our simulation analysis in the 2D model showed that cell morphology and packing are influenced by geometric constraints. Extending this to 3D, we confirmed that

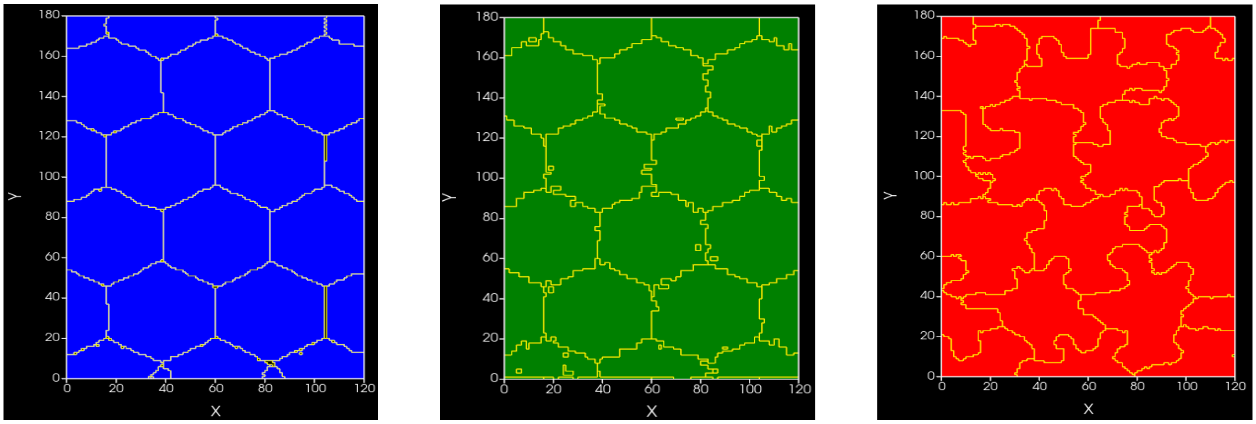

(a) Apical (b) Lateral (c) Basal

Figure 5.2 This image illustrates the XY plane of the three cellular layers after 150 Monte Carlo steps, showcasing the RPE cells morphology across layers. (a) shows the apical cells in a tight end-to-end hexagonal packing, maintaining a highly structured and orderly arrangement. (b) reveals the lateral cells with a wiggling surface. and (c) captures the basal cells where significant interdigitation has occurred, highlighting their complex and interdigitated boundaries.

while geometric constraints limit cell morphology, they are not solely responsible for interdigitation and infolding within the basal cells. Differences in adhesion properties also cause significant variations in cellular morphology and organization. The interplay between adhesion properties and geometric constraints results in the observed interdigitation patterns, demonstrating that changes in these constraints can lead to different cellular behaviors, such as interdigitation in the case of CECs observed in (14) and infoldings described in RPE cells (13).

5.1 Significance of the other Variables within the system's dynamics

This section details how the other parameters within the model affect the dynamics of the system. In the biomechanism process explained in the study, the major parameter explored due to the focus of the study was solely based on the effect of adhesion and perimeter in 2D while the 3D featured the effect of adhesion and 3D. However, there is need to explain how variations in the other parameters affects the dynamics of the system.

5.1.1 Effect of other variables in the 2D model

In section 2, the governing energy equation for the 2D model is defined as:

$$E = \sum_{(i,j)} J_{\tau(\sigma_i),\tau(\sigma_j)} \left(1 - \delta(\sigma_i, \sigma_j)\right) + \lambda_a \sum_{\sigma} \left(a(\sigma) - A_{\text{target}}(\sigma)\right)^2 + \lambda_p \sum_{\sigma} \left(p(\sigma) - P_{\text{target}}(\sigma)\right)^2 \tag{5.1}$$

where $\sum_{(i,j)} J_{\tau(\sigma_i),\tau(\sigma_j)} \left(1 - \delta(\sigma_i, \sigma_j)\right)$ is the differential adhesion, $\lambda_a \sum_{\sigma} \left(a(\sigma) - A_{\text{target}}(\sigma)\right)^2$ represents the area conservation and $\lambda_p \sum_{\sigma} \left(p(\sigma) - P_{\text{target}}(\sigma)\right)^2$ is the cortical tension. From the energy equation of the differential adhesion, the kronecker delta function δ for the cells provided in this study are all of the same type which implies that the nearest neighbour of each cell are all i^{th} cell. As a result, the first term of equation (5.1) results into zero. This implies that the adhesion between the boundaries of the cells is affected by the change in the perimeter. As such, the effective energy of the cell's surface, E_c is proportional to its perimeter as highlighted by (21). Hence, $E_c = \sum_{i=1}^{N} JP_i$.

Similarly, from the area conservation energy, the tuning parameter A_{target} have no effect on the dynamics of the system. This is because of reasons which include the fact that the cells are in confluence without any space for cell growth with an addition of a periodic boundary condition which overcomes the boundary effect meaning that each cell's actual area is preserved throughout the simulations. Thus, the dynamic of the system is independent of the A_{target} and hence leaves the dynamics of the systems to be defined by P_{target}.

5.1.2 Effect of other variables in the 3D model

In the 3D energy function in equation (2.9), five parameters including the adhesion, J; the target surface area, S_{target}; the target cell volume, V_{target} and the Lagrange multipliers λ_s and λ_v describes the cell properties.

Unlike in the 2D model, simulation analysis in the 3D models revealed that all the five (5) parameter play a role in the morphology of the cell. The role of adhesion and its interplay with the surface area of the cell has been explicitly explained as it played the vital role in the formation of interdigitation within the basal cells. In addition to this, our simulation analysis revealed that the volume and the Langrange multipliers are also effective and important. $E_v = \lambda_v \sum(v(\sigma) - V_{target})^2$ describes how the cell's internal pressure is preserved and how it deviates from the V_{target}. An increase in V_{target} causes a corresponding increase in the cell's size and vice versa. λ_v and λ_s affects the balance between maintaining cell shape and allowing deformations which is necessary for the deformation of the cells. As such, an increase in these multipliers causes stiffness within the cell boundaries thereby slowing down the deformation processes but at the same time ensures a tight cell packing.

5.2 Biological Implication

This study has provided a foundation for the comprehensive understanding of RPE cell morphology by extending its morphometric analysis from 2D to 3D, capturing the complex interactions and dynamics that occur in the cell, most especially the biophysical mechanism involved in the interdigitation of the basal cell. Most adhesion complexes explained in textbooks do not fully capture the dynamic and complex nature of cell-cell and cell-matrix interactions observed in this study which are relevant to shape changes in RPE cells. The model demonstrates that disruptions in the balance of cell adhesion and geometric constraints can result in abnormal RPE morphology, which may compromise the supportive role of RPE cells in maintaining photoreceptor health and lead to the progression of AMD.

5.3 Limitations and Future Research

Our computational model is limited by several factors which include a primary focus on the basal interdigitation of the RPE cell, overlooking other important aspects of RPE cell morphology and functions such as those involving apical and lateral surfaces may not be fully captured or understood within the current model framework. In addition, the model's findings are based on computational simulations, and experimental validation is limited. Further experimental studies are needed to validate and refine the model, ensuring that the simulated behaviors accurately reflect real biological processes.

REFERENCES

[1] Bennis A. A quest for the best retinal pigment epithelium (stem) cell replacement therapy., 2017.

[2] Wikipedia contributors. Retinal pigment epithelium — Wikipedia, the free encyclopedia. 2024. [Online; accessed 19-June-2024].

[3] Shreya Somasundaran, Ian J Constable, Carla B Mellough, and Livia S Carvalho. Retinal pigment epithelium and age-related macular degeneration: a review of major disease mechanisms. *Clinical & Experimental Ophthalmology*, 48(8):1043–1056, 2020.

[4] Dry macular degeneration - symptoms and causes - mayo clinic. (Accessed on 06/19/2024).

[5] David B. Rein, John S Wittenborn, Zeb Burke-Conte, Rohit Gulia, Toshana Robalik, Joshua R. Ehrlich, Elizabeth A. Lundeen, and Abraham D. Flaxman. Prevalence of Age-Related Macular Degeneration in the US in 2019. *JAMA Ophthalmology*, 140(12):1202–1208, 12 2022.

[6] Kari V Vienola, Min Zhang, Valerie C Snyder, José-Alain Sahel, Kunal K Dansingani, and Ethan A Rossi. Microstructure of the retinal pigment epithelium near-infrared autofluorescence in healthy young eyes and in patients with amd. *Scientific Reports*, 10(1):9561, 2020.

[7] Peninsula Laser Eye Medical Group. Macular degeneration and nutrition center. https://lasik2020.com/macular-degeneration-nutrition-center/, 2020. (Accessed on

06/19/2024).

[8] Opthalmic Physicians Incorporated. How macular degeneration (armd) affects vision. https://opivision.com/about-us/insights/how-macular-degeneration-armd-affects-vision/. (Accessed on 06/19/2024).

[9] Shagun K Bhatia, Alia Rashid, Micah A Chrenek, Qing Zhang, Beau B Bruce, Mitchel Klein, Jeffrey H Boatright, Yi Jiang, Hans E Grossniklaus, and John M Nickerson. Analysis of rpe morphometry in human eyes. *Molecular vision*, 22:898, 2016.

[10] Yong-Kyu Kim, Hanyi Yu, Vivian R Summers, Kevin J Donaldson, Salma Ferdous, Debresha Shelton, Nan Zhang, Micah A Chrenek, Yi Jiang, Hans E Grossniklaus, et al. Morphometric analysis of retinal pigment epithelial cells from c57bl/6j mice during aging. *Investigative ophthalmology & visual science*, 62(2):32–32, 2021.

[11] Yi Jiang, Xin Qi, Micah A Chrenek, Christopher Gardner, Jeffrey H Boatright, Hans E Grossniklaus, and John M Nickerson. Functional principal component analysis reveals discriminating categories of retinal pigment epithelial morphology in mice. *Investigative ophthalmology & visual science*, 54(12):7274–7283, 2013.

[12] Micah A Chrenek, Nupur Dalal, Christopher Gardner, Hans GrossniklausGrossniklaus, Yi Jiang, Jeffrey H Boatright, and John M Nickerson. Analysis of the rpe sheet in the rd10 retinal degeneration model. In *Retinal Degenerative Diseases*, pages 641–647. Springer, 2012.

[13] Maximilian Lindell, Deepayan Kar, Aleksandra Sedova, Yeon Jin Kim, Orin S Packer, Ursula Schmidt-Erfurth, Kenneth R Sloan, Mike Marsh, Dennis M Dacey, Christine A

Curcio, et al. Volumetric reconstruction of a human retinal pigment epithelial cell reveals specialized membranes and polarized distribution of organelles. *Investigative Ophthalmology & Visual Science*, 64(15):35–35, 2023.

[14] Zhiguo He, Fabien Forest, Philippe Gain, Damien Rageade, Aurélien Bernard, Sophie Acquart, Michel Peoc'h, Dennis M Defoe, and Gilles Thuret. 3d map of the human corneal endothelial cell. *Scientific reports*, 6(1):29047, 2016.

[15] Harold Fernando Gomez, Mathilde Sabine Dumond, Leonie Hodel, Roman Vetter, and Dagmar Iber. 3d cell neighbour dynamics in growing pseudostratified epithelia. *Elife*, 10:e68135, 2021.

[16] James A Glazier, Ariel Balter, and Nikodem J Popławski. Magnetization to morphogenesis: a brief history of the glazier-graner-hogeweg model. *Single-cell-based models in biology and medicine*, pages 79–106, 2007.

[17] Anja Voss-Böhme. Multi-scale modeling in morphogenesis: a critical analysis of the cellular potts model. 2012.

[18] Walter de Back Anja Voss-Böhme, Jörn Starruß. Cellular potts model. https://www2.htw-dresden.de/~avossb/files/Essay-CPM-preprint.pdf. (Accessed on 06/21/2024).

[19] Marco Scianna and Luigi Preziosi. Multiscale developments of the cellular potts model. *Multiscale Modeling & Simulation*, 10(2):342–382, 2012.

[20] Wikipedia contributors. Compucell3d — Wikipedia, the free encyclopedia, 2023. [Online; accessed 21-June-2024].

[21] Souvik Sadhukhan and Saroj Kumar Nandi. Theory and simulation for equilibrium

glassy dynamics in cellular potts model of confluent biological tissue. *Physical Review E*, 103(6):062403, 2021.

[22] Ramiro Magno, Verônica A Grieneisen, and Athanasius FM Marée. The biophysical nature of cells: potential cell behaviours revealed by analytical and computational studies of cell surface mechanics. *BMC biophysics*, 8:1–37, 2015.